Wind Direction Estimation from SAR Images of the Ocean Using Wavelet Analysis

Yong Du*, Paris W. Vachon, John Wolfe

Natural Resources Canada, Canada Centre for Remote Sensing
588 Booth Street, Ottawa, Ontario K1A 0Y7 Canada
Phone: 613 995-2466 / 995-1575 / 995-4913
Fax: 613 947-1385
Email: Yong.Du / Paris.Vachon / John.Wolfe@ccrs.nrcan.gc.ca

27 September 2001

Abstract

We present a method for the automatic estimation of wind directions from SAR images of the ocean. The method is based upon a wavelet analysis and assumes that the wind direction aligns with boundary layer atmospheric roll vortices, which often appear as streaks at kilometre-scales in SAR images of the ocean, and measures the orientation of the streaks. Unlike estimation methods that use the Discrete Fourier Transform (DFT), the streaks in SAR images are described quantitatively as a natural output of this method. Furthermore, more optimal wind directions are obtained by comparing the directional orientation of the streaks at different spatial scales. Sub-scenes in which the streaks are too weak to determine wind direction do not return a wind direction, as governed by a user-selected threshold. Wind directions for these sub-scenes are based upon those in neighbouring sub-scenes by using an adaptive smoothing technique. Quality control involves tuning the threshold level. We apply the method to two examples of RADARSAT-1 SAR images. The results are compared with those of a DFT-based wind direction analysis and it is shown that a robust wind direction field is obtained. Mesoscale wind structures can be described by using a finer computing grid. The estimated wind directions still include a 180° direction ambiguity.

*Under contract to CCRS from Noetix Resaerch Inc., 265 Carling Ave., Suite 403, Ottawa, Ontario K1S 2E1 Canada.

Introduction

Ocean surface wind vector information plays an important role in diverse research and application fields. Wind stress is one of the main forces driving ocean dynamic processes. A detailed description of the wind field structure can improve our understanding of atmospheric processes. Wind is also one of the primary forms of energy exchange between the ocean and the atmosphere. *In situ* data and numerical modeling can provide wind information, but they may be limited by resolution, accuracy, and cost. Synthetic Aperture Radar (SAR) provides an image of the roughness distribution on the sea surface under all weather conditions, with large dynamic range, high accuracy, and high resolution. Retrieval of wind information from SAR images provides a useful complement to support traditional wind observations and numerical modeling.

Wind vector retrieval from SAR images of the ocean has already been shown to be feasible (*e.g.*, Vachon and Dobson, 1996; Wackerman *et al.*, 1996). Wind direction estimation amounts to measuring the orientation of boundary layer rolls in the SAR image. The rolls are often visible as image streaks for higher wind and/or unstable atmospheric conditions (Gerling, 1986; Levy, 2001). The ocean surface wind direction (to within a 180° direction ambiguity) is assumed to lie essentially parallel to the roll or image streak orientation. SAR images of boundary layer rolls are quite variable in terms of roll scale (ranging from 1 to 10's of kilometres) and characteristics (ranging from well defined image streaks to semi-circular, convective cells).

One approach to streak orientation estimation is through spectral analysis of the SAR image with a Discrete Fourier Transform (DFT) (*e.g.*, Wackerman *et al.*, 1996; Vachon and Dobson, 1996). In many cases, the DFT method works well, but the image streaks are not described quantitatively. In addition, when the long-wavelength spectrum is nearly symmetrical, the DFT cannot provide a reliable wind direction (Vachon and Dobson, 1996). The derived wind direction is perpendicular to the peak of the low wavenumber portion of the image spectrum.

Wind speed estimation from SAR images is usually based upon a scatterometer wind retrieval model such as the CMOD (C-band Model) series for VV polarization radars. These models relate the observed radar cross section to the wind speed if the relative wind direction and geometry are known. This approach requires a well-calibrated SAR image.

It has been shown that the wind direction estimated from VV polarization ERS SAR images are within an RMS error of ±19° of *in situ* observations, which in turn results in an RMS wind speed error of ±1.2 *m/s* for CMOD4 (Wackerman *et al.*, 1996). On the other hand, the wind directions estimated from HH polarization RADARSAT-1 SAR images are within an RMS error of ±24° of *in situ* observations, which in turn results in an RMS wind speed error of ±2.4 *m/s* for CMOD_IFR2 with a Kirchhoff polarization ratio (Vachon and Dobson, 2000). The availability of a more reliable and robust technique for wind direction estimation from SAR images will, in turn, lead to improvements in wind speed estimation from SAR images using CMOD-type model functions.

Wavelet analysis is a relatively new mathematical method that is still developing rapidly. Wavelets are inherently tied to the concept of multi-scale analysis. Using wavelets, an image can be depicted as an approximation in overall shape and details that range from relatively broad to rather narrow. This ability to zoom-in or zoom-out that is characteristic of multi-scale analysis permits an image to be interpreted as a sum of the details that appear at different scales. Furthermore, different types of structures in the image may dominate each scale. Wavelet transforms can also be used for edge and feature detection (*e.g.*, Liu *et al.*, 1997), and texture analysis (*e.g.*, Castelman, 1996). The Discrete Wavelet Transform (DWT) naturally describes directional features at different spatial scales in an image, which provides an interesting approach to wind direction estimation from SAR image streaks.

We present a method for the automatic and objective measurement of SAR image streaks that uses wavelet analysis. The Wind Direction from Wavelet Transform (WDWaT) algorithm can quantitatively describe the image streaks through the Standard deviation of the Mean cross-section (*StdM*) of the vertical detail within a wavelet decomposition. The *StdM* can also be used to provide quality control for wind direction estimation. An adaptive smoothing technique was developed to provide an overall continuous and reasonable wind field.

In the next section we discuss wavelet analysis of texture such as streaks in SAR images and introduce the WDWaT algorithm. We then show results from the application of this algorithm in comparison to a DFT approach and for a SAR image of a storm system.

Wavelet-based Texture Analysis

1. Image decomposition and wavelet analysis

We first discuss the discrete one-dimensional wavelet transform (*e.g.*, Castelman, 1996). Let $\mathbf{L}^2(\mathbf{R})$ denote the vector space of a measurable, square-integrable, one–dimensional function $f(x)$. The multi-scale wavelet decomposition is an increasing sequence of closed subspaces $\{V_j\}$ $j \in \mathbf{Z}$ which approximate $\mathbf{L}^2(\mathbf{R})$, where $\mathbf{Z}$ and $\mathbf{R}$ denote the set of integers and real numbers, respectively. In decomposing the signal $f(x)$, the scales are reduced by a factor of 2 for each level by using a scaling function $\phi(x)$. The difference in signal at scales 2^{j+1} and 2^j can be extracted on a wavelet orthonormal basis of $\mathbf{L}^2(\mathbf{R})$. The wavelet function is given by $\psi(x)$, and the wavelet representation is the orthogonal complement of the original signal space, V_2^j, denoted as W_2^j. The decomposition is composed of a new signal approximation and a detail signal. The signal approximation is given by

$$\hat{f}_{2^j}(x) = \sum_k \left\langle \phi_{2^{-1}}(x), \phi(x-(k-2n)) \right\rangle \left\langle f(x), \phi_{2^{j+1}}(x-2^{-j-1}k) \right\rangle \tag{1}$$

where $k \in \mathbf{Z}$ and $\langle a,b \rangle$ is the inner product of a and b. The scale change is obtained by the first inner product which acts as a low pass filter: *i.e.*,

$$h(n) = \left\langle \phi_{2^{-1}}(x), \phi(x-n) \right\rangle \tag{2}$$

and by sub-sampling by a factor of two. Using Equation (2), Equation (1) becomes

$$\hat{f}_{2^j}(x) = \sum_k \widetilde{h}(2x-k)\hat{f}_{2^{j+1}}(k) \tag{3}$$

where $\widetilde{h}(n) = h(-n)$.

Similarly, the detail signal from the orthogonal projection of $f(x)$ onto W_2^j is given by

$$d_{f_{2^j}}(x) = \sum_k \left\langle \psi_{2^{-1}}(x), \phi(x-(k-2n)) \right\rangle \left\langle f(x), \phi_{2^{j+1}}(x-2^{-j-1}k) \right\rangle. \tag{4}$$

The detail difference between scales is obtained by the first inner product, which acts as a high pass filter:

$$g(n) = \langle \psi_{2^{-1}}(x), \phi(x-n) \rangle \tag{5}$$

where $g(n)$ is the quadrature mirror filter of $h(n)$. Using Equation (5), Equation (4) becomes

$$d_{2^j}(x) = \sum_k \tilde{g}(2x-k) \hat{f}_{2^{j+1}}(k) \tag{6}$$

where $\tilde{g}(n) = g(-n)$. Thus, the signal approximation at the next lower scale ($j+1 \rightarrow j$) is decomposed into a low pass approximation and a high pass detail signal (*i.e.*, the wavelet coefficients).

Perfect reconstruction of the original signal, $f_{2^{j+1}}(x)$, requires that the filters $h(n)$ and $g(n)$ have regularity constraints (Daubachies, 1988). The reconstruction is the inverse wavelet transform that takes the form of

$$\hat{f}_{2^{j+1}}(x) = \sum_k \tilde{h}(2k-x) \hat{f}_{2^j}(k) + \tilde{g}(2k-x) d_{f_{2^j}}(k) \tag{7}$$

The discrete two-dimensional wavelet transform is a straightforward extension of the one-dimensional wavelet transform, which can be interpreted as two one-dimensional wavelet transforms along both the x and y axes (Mallat, 1989). As in the one-dimensional case, the original image is reduced in scale by a low-pass filter and sub-sampling to form an approximation image, but this time it is for both the rows and columns of the image. This is a separable multi-scale approximation of $\mathbf{L}^2(\mathbf{R}^2)$ in which the scaling function is

$$\Phi(x, y) = \phi(x)\phi(y). \tag{8}$$

The resulting two-dimensional decomposition at a given scale results in three detail images that are a set of independent, spatially oriented frequency channels that detail vertical high frequencies, horizontal high frequencies, and cross-directional high frequencies (see Fig. 1). The three wavelets that give these detail images are

$$\begin{aligned}
\Psi^V(x, y) &= \phi(x)\psi(y), \\
\Psi^H(x, y) &= \psi(x)\phi(y), \\
\Psi^D(x, y) &= \psi(x)\psi(y).
\end{aligned} \tag{9}$$

From Equation (9), it is known that the three details at specific scales describe different directional features at this scale. The first one, $\Psi^V(x, y)$, works as a filter with vertical high-pass and horizontal low-pass. Therefore, it mainly enhances and describes the vertical features at a certain scale in the image. Similarly, $\Psi^H(x, y)$ and $\Psi^D(x, y)$ can be used to describe the horizontal and diagonal features at the same scale. The original image in Fig. 1 contains distinct, vertically oriented striped features. From the decomposition at scales 1 and 2, it can be seen that the vertical detail contains the stronger vertical stripes. The horizontal and diagonal details are much weaker. These orientation properties of the wavelet analysis can be applied to the detection, enhancement, and description of directional features of images at different scales.

2. Estimation of directional features in SAR images

Wind direction retrieval is based on the measurement of texture features in SAR images of the ocean. A texture feature is a value, computed from a whole image or a sub-scene, which quantifies some characteristic of the grey-level variation within the immediate area. Therefore, it is a spatial concept that is related to the scale of the computation area. Roughly, SAR image textures can be classified as random or pattern textures. Random textures are characterized by statistical properties such as the standard deviation of the grey-level (for measuring the amplitude of the texture) and the auto-correlation function width (for measuring the spatial scale of the texture). Speckle noise in SAR images is an example of a random texture. Pattern textures can be additionally characterized by extracting measurements that quantify the nature and directionality (if any) of the pattern. The streaks in SAR images that are related to wind direction are examples of pattern textures.

For estimating the relative strength of the streaks in SAR image, we introduce the Maximum of the Standard deviations of the Mean cross-section (*MStdM*) as a detection criterion. The cross-section mean of the area of interest is obtained by computing the mean value of each column in a vertical direction (see Fig. 2a). When the image is rotated through 180° with a given rotational interval, the mean values of the cross-section at different angles are obtained (Fig. 2b). The rotation angle interval is $180°/n$ ($180 > n > 1$) and the choice of n depends on the accuracy of estimation that is required, and proportionally scales the computation cost. After a complete rotation, n curves of the cross-section mean value are obtained. The *MStdM* and the Average of the Standard deviations of the Mean cross-section (*AvStdM*) of these curves are calculated as:

$$MStdM = max\ [StdM(1), StdM(2), \ldots , StdM(n)]$$

$$AvStdM = average\,[StdM(1), StdM(2), \ldots, StdM(n)] \tag{10}$$

where *MStd(i)* is the Standard deviation of the Mean cross section for the i^{th} rotation angle. We introduce the factor *k* to describe the strength of the directional features:

$$k = \frac{MStdM}{AvStdM} \geq 1 \tag{11}$$

The higher the value of *k,* the stronger the directional features in the image. With a given threshold, *k* can be used to make a quality control decision. When *k* is higher than a user-defined threshold, the surface feature in the image may be considered to be directional; otherwise, it is too weak to extract a reliable direction. The threshold can be given based on specific cases and the analyst's experience. For an image area containing streaks, the most likely direction of the texture is the direction of the *MStdM* derived from the rotation angle. If the north direction is zero and the rotation is clockwise, then the direction of the streaks is equal to the negative rotation angle of the *MStdM*.

3. Extraction of streaks at multi-scales with wavelet texture analysis

In the previous sub-section, a criterion was introduced for the estimation of streaks in SAR images. The estimated direction is from the texture features with all wavelengths or spatial scales. However, the wind direction is normally following kilometre-scale features under specific stability and wind speed conditions. Thus, the texture features at various scales should be separated, and the kilometre-scale features should be analyzed individually for estimation of the wind direction. This naturally leads to a wavelet multi-scale analysis.

With the two-dimensional discrete wavelet transform, a SAR image can be decomposed into different scale images, which describe different scale texture features. The scale of the decomposition depends on the scale of the texture features of interest, the pixel spacing, and the size of the original image. For example, if the pixel spacing of a RADARSAT-1 ScanSAR wide mode image is 50 *m*, scale 1, 2, 3, 4, 5, and 6 decompositions of the image will contain the spatial variations or texture features of $50\ m \times 2^1 = 0.1\ km$, … , $50\ m \times 2^5 = 1.6\ km$, and $50\ m \times 2^6 = 3.2\ km$ wavelengths, respectively.

At each scale of the decomposition with a two-dimensional discrete wavelet transform, there are four components: one approximation and three details. It has already been noted that the vertical detail describes and enhances the vertical features at a specific individual scale (Fig. 1). The principle of directional estimation is that the vertical features should be the strongest when the direction of the image streak is aligned with the vertical direction. Therefore, the vertical detail image at the scale of interest could be used as a basic template for the detection and estimation of directionally oriented features in SAR images. Rotating the SAR image and computing the vertical detail at a particular scale can extract the streak information for different angles. For the individual scale, the extraction rule is that the direction of the texture feature must be aligned with the maximum vertical *StdM* at that scale. Under this rule, the directions of streaks at different scales can be found. *MStdM* and *AvStdM* can also be calculated at different spatial scales by using Equation (10). The directional factor k at different scales can be obtained from Equation (11).

Compared to a traditional texture analysis, the superiority of a wavelet-based texture analysis is that multi-scales are used. The different scales of the streaks allow the directional information to be extracted in more detail. The directional factor k at different scales can tell us at which scale the spatial feature is the most directional. Therefore, the directional factor k is the key to determining the optimal spatial scale for the directional estimation of texture features.

Fig. 3a shows an example for a 256×256 pixel sub-scene of rotated vertical detail at a scale of 3.2 *km*. Fig. 3b is the cross-section mean curves rotated from 0° to 170° with an interval of 10°. The *StdM*'s of vertical detail, *MStdM* and *AvStdM* are provided in Table 1. *MStdM* = 1.17 at a rotation angle of 20°; *AvStdM* = 0.33; and k = 3.55. In this case, therefore, the direction of the streak feature is –20° with k = 3.55.

4. Automatic estimation of wind direction with quality control

Several sources of wind directions have been used in the estimation of the wind vectors from SAR images of the ocean, such as from numerical models and image spectral analysis (Vachon and Dobson, 1996; Thompson and Beal, 2000; Horstmann *et al.*, 2000; Vachon and Dobson, 2000). Here, we introduce the procedure WDWaT, an application of wavelet multi-scale analysis presented in the last sub-section, to automatically estimate the wind direction from streak orientation in SAR images of the ocean.

The calculated *MStdM*'s and *AvStdM*'s of the vertical detail images at different scales are used to calculate the directional factor k at each individual scale. Because the wind direction is extracted from the kilometre-scale (from 0.5 to 20 *km*, say) texture features in SAR images, several directional factors at different scales may be calculated to find the optimal scale. For an automatic procedure, all scales (for example, 0.5, 1, 2, 4, 8, and 16 *km*) could be included in the calculation. The values of k at different scales are then compared. The scale with the highest value of k is the optimal scale of the directional feature. The wind direction is then taken as the orientation of the directional feature at the optimal scale. When the maximum value of k for all scales is less than a user-defined threshold, the feature is considered to be too weak to reliably estimate the streak orientation, and may be eliminated from the grid. However, the missing wind direction value may be estimated from the neighbouring wind directions in the grid as a separate step.

Further quality control of the estimated grid of wind directions is based on wind field coherence. After the wind direction is estimated from the texture features at the different scales for the overall wind field, the relation between each grid point and the neighbouring points should be considered. The assumption is that the spatial variation of the wind direction is smooth, or changes gradually; no single wind direction should be beyond a given variation limit when compared with the mean or median wind direction in the local neighbourhood. In this kind of quality control, two factors should be considered: first, the impacted coverage; and second, the variation limit. A moving boxcar window may be used to adjust the overall wind direction field. The wind direction at the central point of the boxcar may be improved by comparing with the mean or median wind direction within the overall boxcar coverage.

In practice, if a SAR image contains only simple feature structures, then the number and range of scales for the calculation can be deduced from visual inspection and the pixel spacing of the image. This could result in a significant savings in computing costs. It should be pointed out that this kind of selection of scale number and range does not affect the automatic property of the WDWaT algorithm. Fig. 4 is a flowchart of WDWaT.

Validation and Applications

Procedures for wind direction estimation may be validated by comparing with reference data such as *in situ* wind vector observations (*e.g.*, Vachon and Dobson, 1996; Wackerman *et al.*, 1996). However, there are several differences between wind directions extracted from a SAR image of the ocean and reference data observed at the sea surface. First, the former is a spatial average while the latter is a temporal average, which means that only when the wind is stable both temporally and spatially would the two wind directions be consistent. Second, an important assumption for the extraction of wind direction from the SAR images of the ocean is that the wind is the sole factor affecting the roughness of the sea surface. However, spatial patterns in actual SAR ocean images may be generated and influenced by many factors, some of which do not depend directly on the actual wind conditions. Third, data pairs are often difficult to synchronize in time and space. If these differences cannot be calibrated, they will impact the wind estimation accuracy.

In this study, the accuracy of extracted wind direction with WDWaT was estimated by comparing with *in situ* wind observations. The variance of the results depends on the selected data pairs, making it difficult to have a reliable, quantitative assessment of the WDWaT and DFT algorithms. Therefore, we are reduced to validating WDWaT wind directions through case studies, which also include comparing with DFT results, and qualitative assessment of the tracking of rather complex meteorological fronts and storm structures.

1. Comparison with DFT

A RADARSAT-1 wide beam mode SAR image was acquired on 27 Feb. 1997 over the Research Vessel *Knorr* off the Labrador Coast (Fig. 5a). The image was first block-averaged by a factor of four from 12.5 *m* to 50 *m* pixel spacings. Wind directions were then calculated using 32 *km* by 32 *km* sub-images on a grid spacing of 20 *km* by 20 *km*. The *StdM* was calculated on a sub-area of 16 *km* by 16 *km*.

Each sub-image was decomposed with ***db*4** wavelet basis, one of the family members of the compact and well-localized wavelets first presented by Daubechies (1988). The wind direction field was then calculated using WDWaT (Fig. 5b) as well as at 2, 4, 8, and 16 *km* scales with the minimum directional factor threshold set to $k = 1.8$. The derived wind directions were then adaptively smoothed with a 3×3 moving boxcar window.

The wind direction arrows that are maximum for selected scales are shown with different colours as indicated in the figure caption. From Fig. 5b, it can be seen that the majority of the wind direction arrows are red and magenta in colour, indicating that the directional features with 16 and 8 *km* scales are dominant. In this case, it is readily apparent that the SAR image contains a simple directional feature of boundary layer atmospheric roll vortices with a rather consistent direction at coarser scales. The automatic selection of the appropriate spatial scale and wind direction using WDWaT is seen to be quite consistent with a visual inspection of the image.

For further illustration, the wind directions were then calculated at the set of individual scales with a wavelet transform (Fig. 5c through 5f). The calculation is under the same conditions as WDWaT except for the selection of the optimum scale. It can be seen that the 16 and 8 *km* scales provide good results in this case, although some details appear to be lost in comparison with WDWaT. The 4 and 2 *km* scales have evidently produced inconsistent results. Therefore, it is apparent that the selection of the spatial scale is critical to the estimation of the wind direction. Because of the good results at the 16 and 8 *km* scales, we conclude that the scale is not a very strict parameter. That is, we expect that the wind direction should be the consistent within similar scales.

For comparison purposes, a wind direction field for the same image was derived using a DFT method. This analysis proceeded by first extracting an image sub-scene and then generating a SAR image spectrum using Welch's method of averaging modified periodograms. The spectrum was then smoothed and an annular portion centred on the DC-component was extracted. The orientation of the image spectrum, and therefore the wind direction, may be found by fitting a 2-dimensional Gaussian-shaped surface, calculating the centre-of-mass of the half plane, by finding the location of the spectral peak, or by finding the principle axes of the low wavenumber spectrum.

To ensure the detection of large-scale image streaks, a sub-scene of 51.2 *km* by 51.2 *km* (corresponding to 4096×4096 pixels) was used. We obtained a 3 (in azimuth) $\times$ 2 (in range) matrix of image spectra from which a total of 6 unique wind directions across the image were estimated. The analyzed portion of the spectrum was restricted to wavelengths greater than 10 *km*; the orientation (major axis) was derived from the centre-of-mass of the half plane.

It can be seen from Fig. 6 that the DFT approach also provided a good result in the case of a consistent wind direction. However, the DFT approach is somewhat subjective since *a priori* knowledge is required to select appropriate sub-image sizes and analysis length scales.

2. Meteorological fronts and storm structures

To further demonstrate the WDWaT algorithm, we considered a RADARSAT-1 ScanSAR wide mode image of a storm that was acquired on 13 Jan. 1999 off the Labrador coast (see Chunchuzov *et al.* (2000) for additional examples of RADARSAT-1 ScanSAR images of high latitude storms). This image is more of a challenge to analyze than the last example because of the complex spatial patterns, including a front and other storm structures. It is apparent that high winds are a major factor controlling the appearance of the image streaks, which are present in this case with several different scales and orientations.

The image was first block-averaged by a factor of four from 50 *m* to 200 *m* pixel spacings. Wind directions were then calculated using 25.6 *km* by 25.6 *km* sub-images on a grid spacing of 20 *km* by 20 *km*. The *StdM* was calculated on a sub-area of 12.8 *km* by 12.8 *km*. In the region of the storm eye, the computation grid was narrowed to 12 *km* by 12 *km* grid in order to better describe the finer structures in more detail.

From Fig. 7, it can be seen that the front and storm structures are well described by the WDWaT algorithm. To the left of the front, finer scale structures are dominant. The optimal scales are 3.2 and 1.6 *km* (blue and green), consistent with visual inspection. To the right of the front, the dominant scales are much coarser at 12.8 and 6.4 *km* (magenta and red). In the eye of the storm, the scales of the features are mixed. Although the 0.8 *km* scale (black) was involved in the calculation, only a few points are dominant at this scale. Therefore, scales of less than 1 *km* are not effective for estimation of the wind direction over the ocean, at least for this particular SAR image. The "+" marks indicate the weak texture locations; most appear in the (dark) areas with relatively low wind speed.

Conclusions

We have proposed and demonstrated the Wind Direction from Wavelet Transform (WDWaT) algorithm for wind direction estimation from streak orientation in SAR images of the ocean. The algorithm takes advantage of the unique properties of wavelet transforms, especially in comparison to the more popular Discrete Fourier Transform (DFT) algorithms, by providing a multi-scale texture analysis. Estimation of wind direction from SAR images of the ocean is a typical multi-scale texture analysis problem to which the wavelet transform is well suited. The Maximum of the Standard deviation of the Mean cross section (*MStdM*) was used to determine the orientation of image streaks.

The WDWaT algorithm has some new and unique characteristics:

- The direction factor *k* was introduced as a quantitative description of the image streaks, which provides the alignment of texture in SAR images and a relative accuracy measurement;
- Multi-scale wavelet texture analysis results in the direction of texture feature analyzed at individual scales;
- The optimal kilometre-scale for wind direction retrieval is selected objectively, which results in an automatic estimation of wind direction from SAR images;
- Sub-scenes of weak directional features are identified and eliminated as an element of quality control;
- Adaptive smoothing techniques improve the overall distribution of wind directions based on the relation among neighbouring grid points.

So far, good wind direction estimation results have been obtained by using the ***db4*** wavelet basis functions. However, a different wavelet basis or wavelet family might produce slightly different results during image decomposition. The selection of the optimal wavelet family and wavelet basis for this application is still under study. It should be noted that wind directions estimated with the WDWaT algorithm still contain an inherent 180° wind direction ambiguity.

References

Castleman, K. R. (1996). *Digital Image Processing*, Prentice Hall, Upper Saddle River, New Jersey.

Chunchuzov, I., P.W. Vachon, and B. Ramsay (2000). Detection and characterization of mesoscale cyclones in RADARSAT synthetic aperture radar images of the Labrador Sea, *Can. J. Rem. Sens.*, **26(3)**: 213-230.

Daubechies, I. (1988). Orthonormal bases of compactly supported wavelets, *Commun. Pure Appl. Math.*, **91**: 909-996.

Gerling, T.W. (1986). Structure of the surface wind field from the Seasat SAR, *J. Geophys. Res.*, **91(C2)**: 2308-2320.

Horstmann, J., W. Koch, S. Lehner, and R. Tonboe (2000). Wind retrivieval over the ocean using synthetic aperture radar with C-band HH polarization, *IEEE Trans. Geoscience Rem. Sens.*, **38(5)**: 2122-2131.

Levy, G. (2001). Boundary Layer Roll Statistics from SAR, *Geophys. Res. Let.*, **28(10)**: 1993-1995.

Liu, A.K., C.Y. Peng, and S.Y-S. Chang (1997). Wavelet analysis of satellite images for Coastal Watch, *IEEE J. Oceanic Eng.*, **22**: 9-17.

Mallat, S.G. (1989). A theory for multiresolution signal decomposition: the wavelet representation, *IEEE Trans. Pattern Anal. Mach. Intell.*, **2**: 674-693.

Thompson, D.R., and R.C. Beal (2000). Mapping High-resolution wind fields using synthetic aperture radar, *Johns Hopkins APL Technical Digest*, **21(1)**: 58-67.

Vachon, P.W., and F.W. Dobson (1996). Validation of wind vector retrieval from ERS-1 SAR images over the ocean, *The Global Atmosphere and Ocean System*, **5**: 177-187.

Vachon, P.W., and F.W. Dobson (2000). Wind retrieval from RADARSAT SAR images: Selection of a suitable C-band HH polarization wind retrieval model, *Can. J. Rem. Sens.*, **26(4)**: 306-313.

Wackerman, C.C., C.L. Rufenach, R.A. Shuchman, J.A. Johannessen, and K.L. Davidson (1996). Wind vector retrieval using ERS-1synthetic aperture radar imagery, *IEEE Trans. Geoscience Rem. Sens.*, **34(6)**: 1343-1352.

<u>List of Tables:</u>

Table 1. Calculated values of the Maximum of the Standard deviations of the Mean cross section (*MStdM*), the Average of the Standard deviations of the Mean cross section (*AvStdM*), and the directional factor *k* for example image of ‘. 3.

<u>List of Figures:</u>

Figure 1. A standard orthonormal decomposition using a wavelet transform with two scale levels. The panels include vertical (V), horizontal (H), and diagonal (D) detail images at scales 1 and 2, as well as the corresponding approximation image (A2).

Figure 2. Calculation of the Standard deviation of the Mean cross section (*StdM*) and for two different rotation angles: (a) 0°; and (b) 20°.

Figure 3. Calculation of the Standard deviation of the Mean cross section (*StdM*) from an image with vertical detail: (a) rotated images (0 to 170°); and (b) *StdM*’s.

Figure 4. Wind Direction from Wavelet Transform (WDWaT) algorithm flowchart.

Figure 5. Comparison of estimated wind direction between Wind Direction from Wavelet Transform (WDWaT) and that at the individual spatial scales: (a) RADARSAT-1 single beam mode image from the *Knorr* campaign off the Labrador coast, acquired 27 Feb. 1997 and covering 137 *km* from left-to-right (© Canadian Space Agency, 1997); (b) wind directions from WDWaT with Red - 16 *km*; Magenta - 8 *km*; Blue - 4 *km*; Green - 2 *km*; “+” - weak; wind directions from Discrete Wavelet Transform at scales of (c) 16 *km*; (d) 8 *km*; (e) 4 *km*; and (f) 2 *km*.

Figure 6. Estimated wind directions using a Discrete Fourier Transform (DFT) algorithm applied to the image of Fig. 5a.

Figure 7. Results of the Wind Direction from Wavelet Transform (WDWaT) algorithm applied to a RADARSAT-1 ScanSAR wide mode image of the Labrador Coast, acquired 13 Jan. 1999 and covering 531 *km* from left-to-right (© Canadian Space Agency, 1999). Red - 12.8 *km*; Magenta - 6.4 *km*; Blue - 3.2 *km*; Green - 1.6 *km*; Black - 0.8 *km*; “+” - weak.

Table 1

Rotation Angle	*StdM*		Rotation Angle	*StdM*
0º	0.33		90º	0.19
10º	0.48		100º	0.18
20º	1.17		110º	0.25
30º	0.56		120º	0.28
40º	0.29		130º	0.25
50º	0.19		140º	0.33
60º	0.15		150º	0.33
70º	0.20		160º	0.26
80º	0.15		170º	0.38
MStdM = 1.17			Max Angle = 20º	
AvStdM = 0.33			*k* = 3.55	

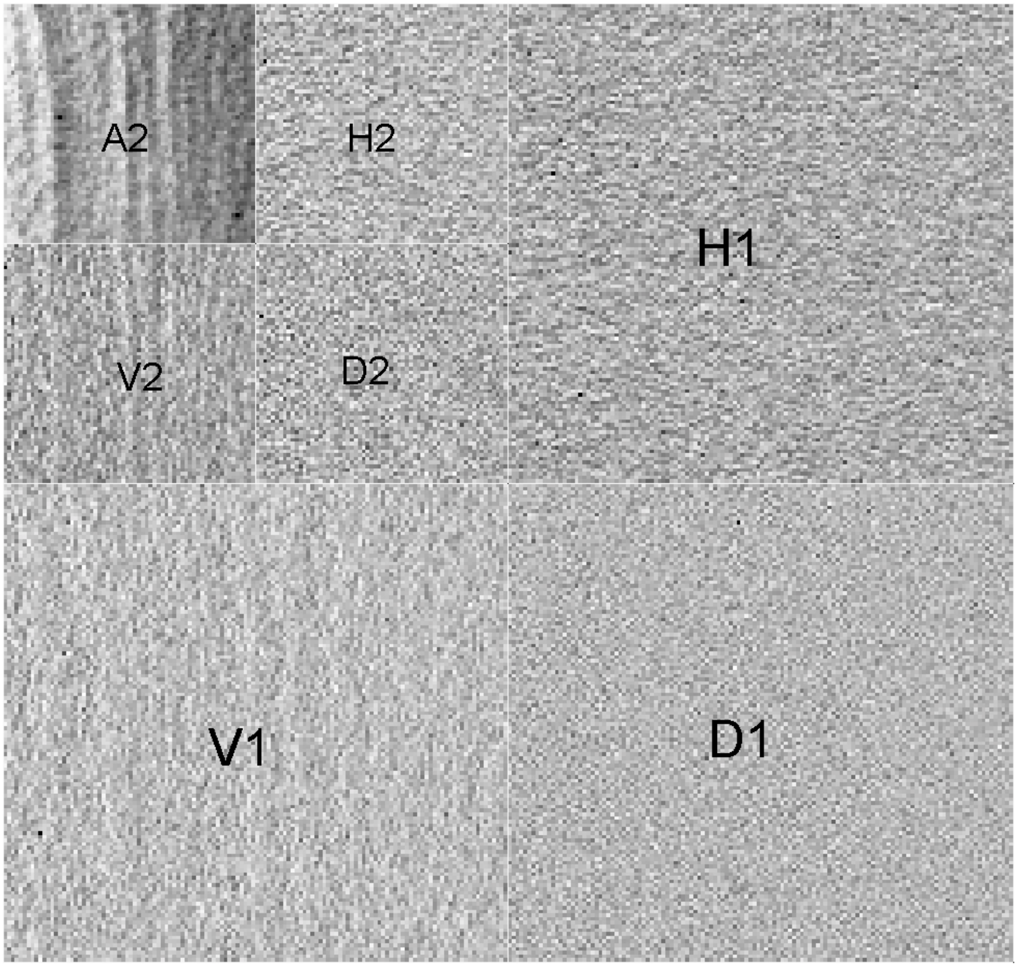

Figure 1

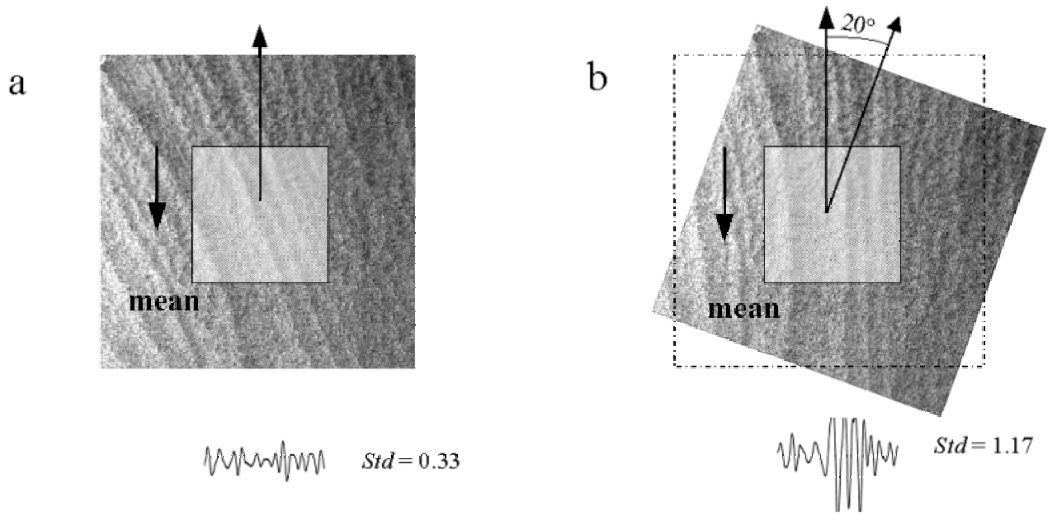

Figure 2

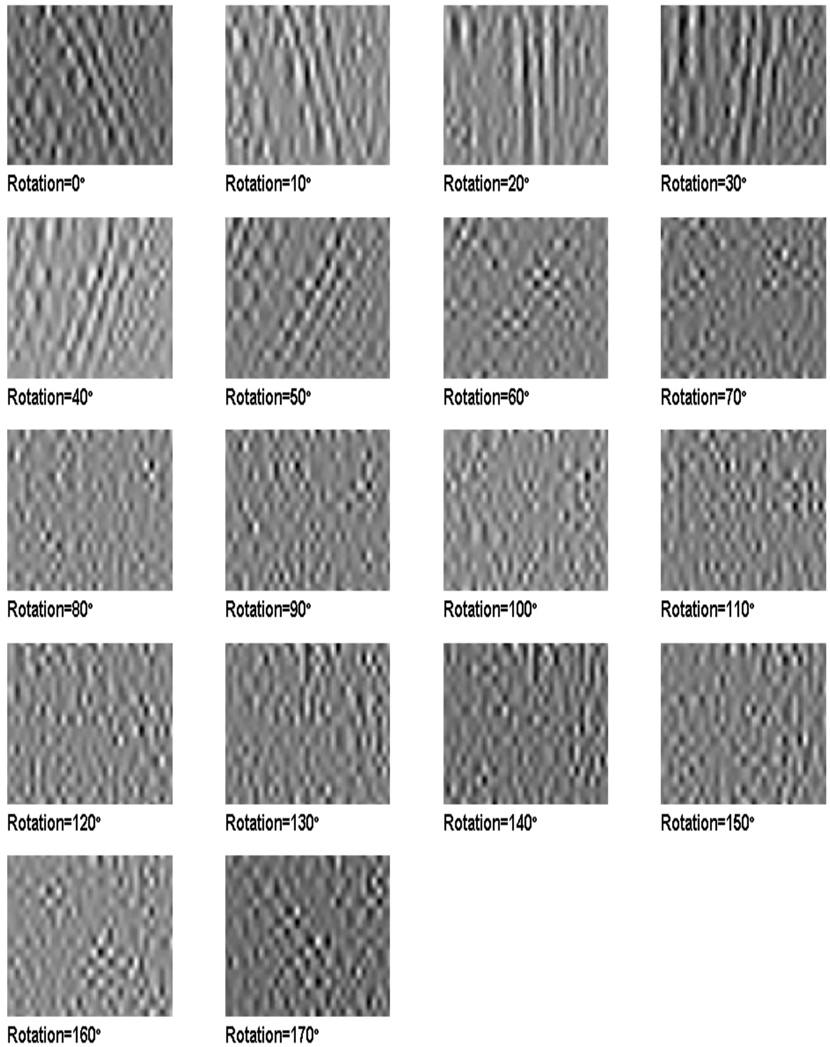
Rotation=0°
Rotation=10°
Rotation=20°
Rotation=30°
Rotation=40°
Rotation=50°
Rotation=60°
Rotation=70°
Rotation=80°
Rotation=90°
Rotation=100°
Rotation=110°
Rotation=120°
Rotation=130°
Rotation=140°
Rotation=150°
Rotation=160°
Rotation=170°

Figure 3a

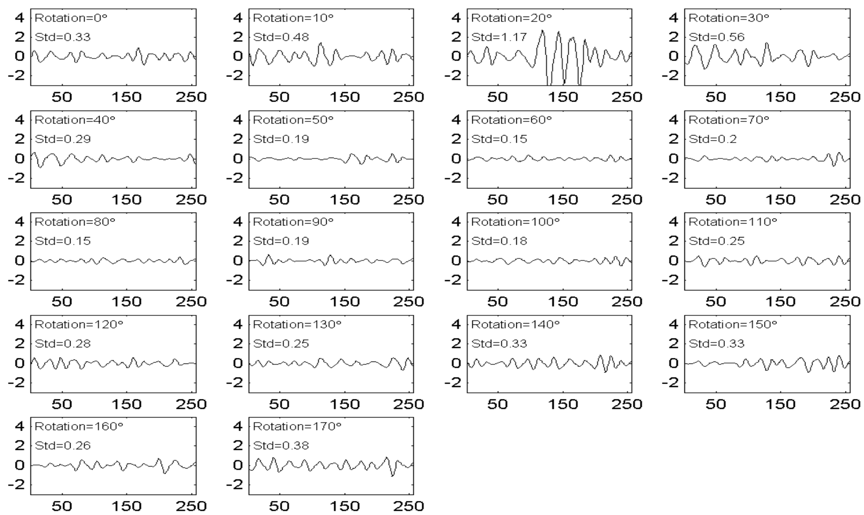
Rotation=0°
Std=0.33
Rotation=10°
Std=0.48
Rotation=20°
Std=1.17
Rotation=30°
Std=0.56
Rotation=40°
Std=0.29
Rotation=50°
Std=0.19
Rotation=60°
Std=0.15
Rotation=70°
Std=0.2
Rotation=80°
Std=0.15
Rotation=90°
Std=0.19
Rotation=100°
Std=0.18
Rotation=110°
Std=0.25
Rotation=120°
Std=0.28
Rotation=130°
Std=0.25
Rotation=140°
Std=0.33
Rotation=150°
Std=0.33
Rotation=160°
Std=0.26
Rotation=170°
Std=0.38

Figure 3b

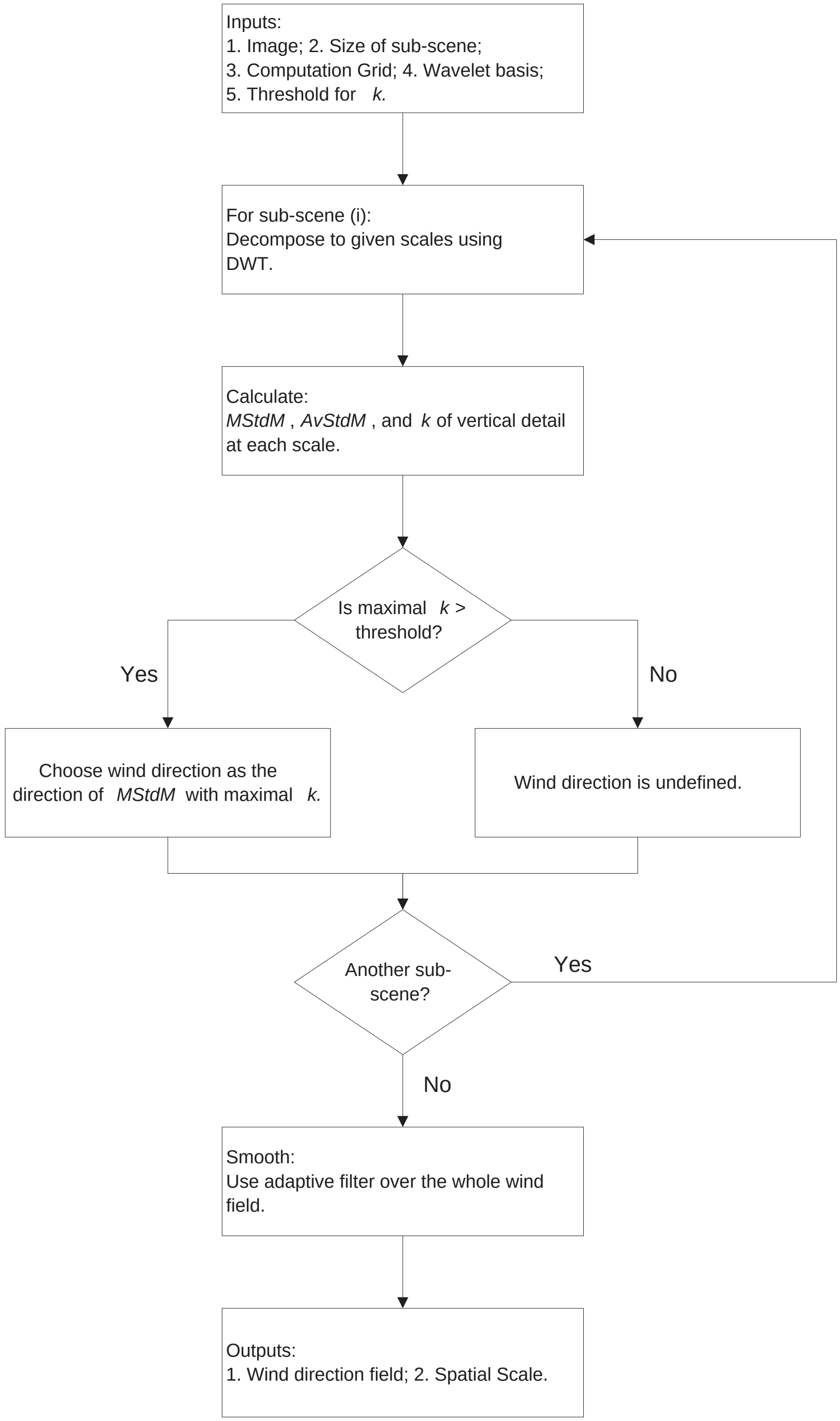
Inputs:
1. Image; 2. Size of sub-scene;
3. Computation Grid; 4. Wavelet basis;
5. Threshold for k.
For sub-scene (i):
Decompose to given scales using DWT.
Calculate:
MStdM , AvStdM , and k of vertical detail at each scale.
Is maximal k > threshold?
Yes
No
Choose wind direction as the direction of MStdM with maximal k.
Wind direction is undefined.
Another sub-scene?
Yes
No
Smooth:
Use adaptive filter over the whole wind field.
Outputs:
1. Wind direction field; 2. Spatial Scale.

Figure 4

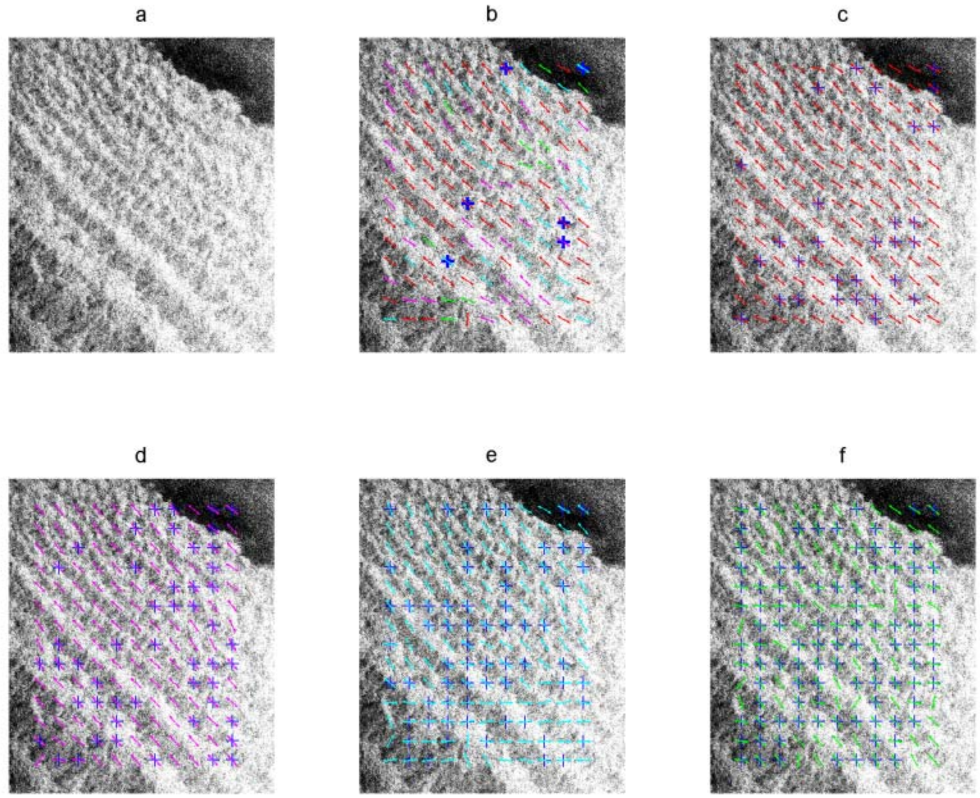

Figure 5

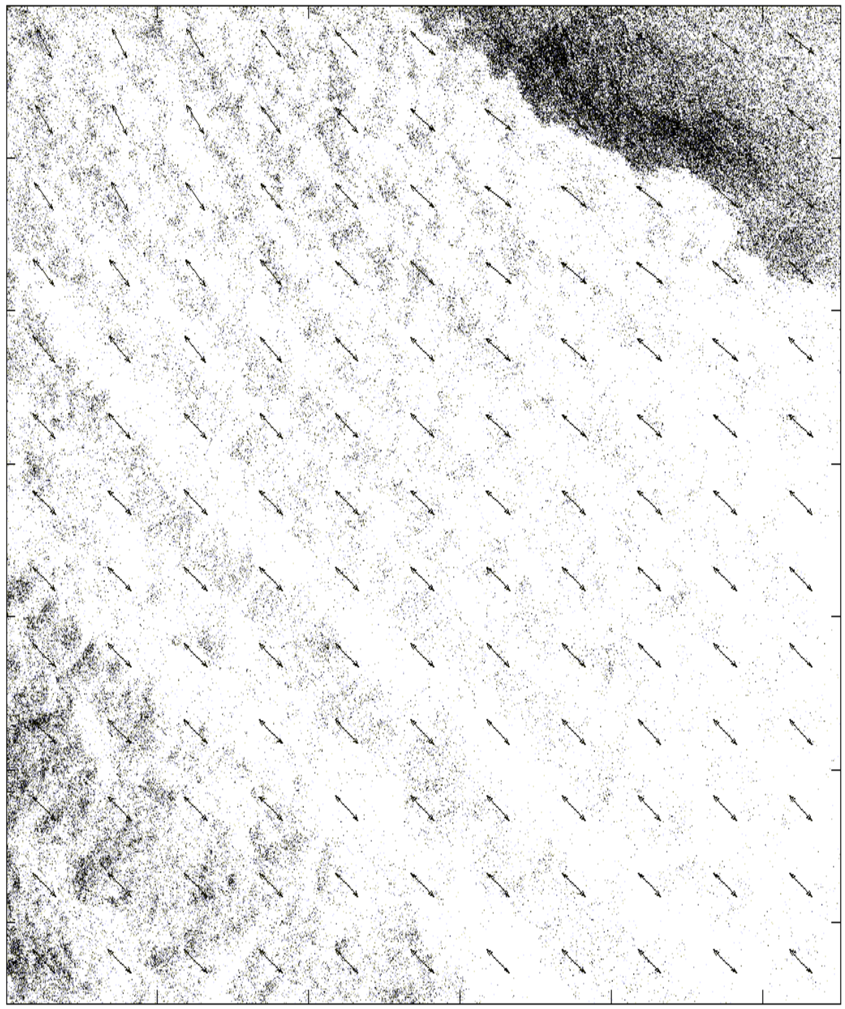

Figure 6

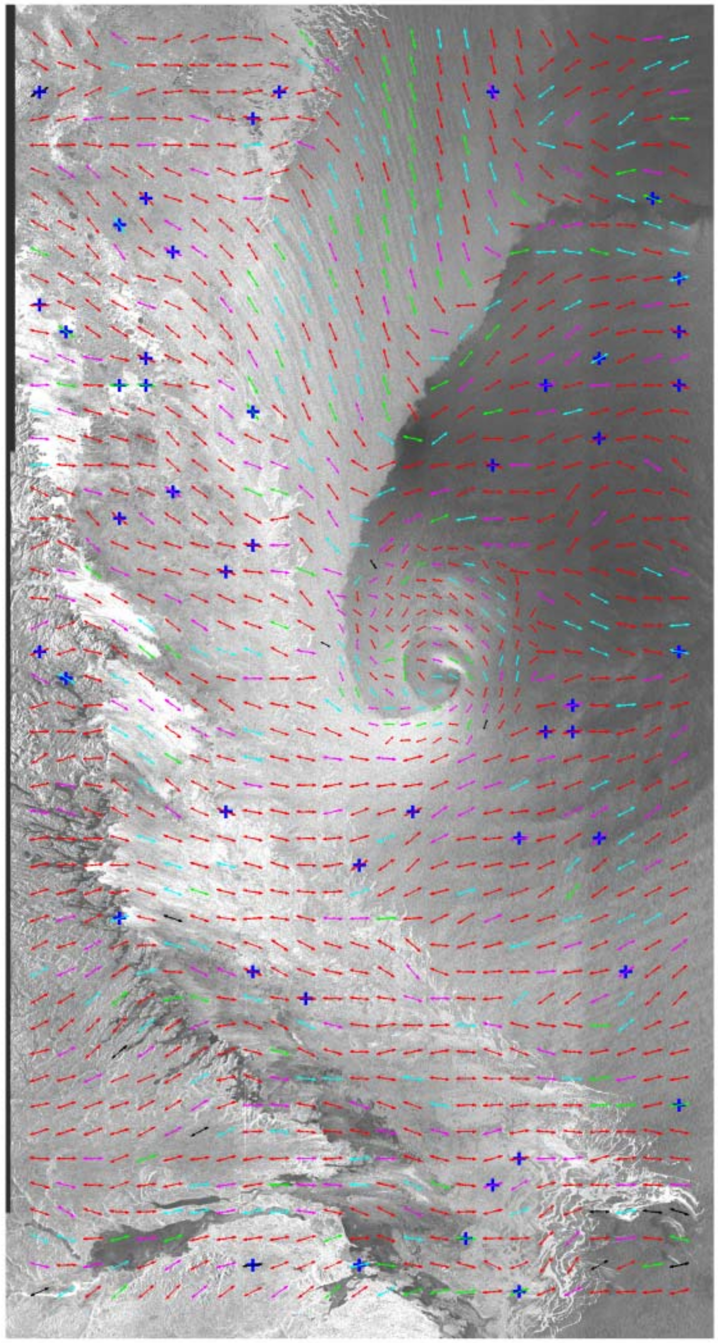

Figure 7